Structural Engineering and Mechanics, *Vol. 69, No. 3 (2019) 283-291*
DOI: https://doi.org/10.12989/sem.2019.69.3.283

Analytical solution for free vibration of multi-span continuous anisotropic plates by the perturbation method

Jiepeng Liu[1,3a], Liang Cao*[1,2,3] and Y. Frank Chen[1,3a]

[1]*School of Civil Engineering, Chongqing University, Chongqing, China*
[2]*Postdoctoral Research Station, School of Civil Engineering, Chongqing University, Chongqing 400045, China*
[3]*Key Laboratory of New Technology for Construction of Cities in Mountain Area (Chongqing University), Ministry of Education, Chongqing 400045, China*

(Received January 31, 2018, Revised October 12, 2018, Accepted November 27, 2018)

Abstract. Accurately determining the natural frequencies and mode shapes of a structural floor is an essential step to assess the floor's human-induced vibration serviceability. In the theoretical analysis, the prestressed concrete floor can be idealized as a multi-span continuous anisotropic plate. This paper presents a new analytical approach to determine the natural frequencies and mode shapes of a multi-span continuous orthotropic plate. The suggested approach is based on the combined modal and perturbation method, which differs from other approaches as it decomposes the admissible functions defining the mode shapes by considering the intermodal coupling. The implementation of this technique is simple, requiring no tedious mathematical calculations. The perturbation solution is validated with the numerical results.

Keywords: perturbation method; multi-span continuous anisotropic plate; intermodal coupling; natural frequencies

1. Introduction

The design of a long-span or lightweight floor is often governed by the vibration serviceability requirement rather than by the strength one (Chen *et al*. 2013, Wang and Chen 2017). This presents a more involved structural assessment. As part of the entire task, the free vibration analysis for a building floor is an essential step for studying the human-induced vibration problem. Such analysis typically requires the determination of natural frequencies and mode shapes. The rectangular floor is usually idealized as an anisotropic plate to investigate the human-induced vibration from walking, running, or other rhythmic movement.

Several methods and techniques have been developed and used to determine the natural frequencies and natural mode shapes of a multi-span continuous anisotropic plate, particularly the analytical ones. For example, Veletsos and Newmark (1956) used the Holzer method for torsional vibration of shafts to determine the natural frequencies of a simply-supported plate. Ungar (1960) developed a simple semigraphical method for calculating the natural frequencies of a two-plate system. Lin *et al*. (1964) and Mercer and Seavey (1967) proposed a transfer matrix method for analyzing a continuous finite plate. Dickinson and Warburton (1967) utilized the edge-effect method to study single- and multi-plate systems. Elishakoff and Sternberg (1979) applied the modified Bolotin method to determine the eigenfrequencies of a continuous rectangular isotropic plate on rigid supports. More recently, the receptance method developed by Bishop and Johnson was exploited by Azimit *et al*. (1984) to study the free vibration of continuous rectangular plates. Gorman and Garibaldi (2006) utilized the superposition method to obtain the frequencies and mode shapes of free vibration for three-span thin plates. Zhou (1994), Zhu and Law (2002), and Marchesiello *et al*. (1999) employed the eigenfunctions of a continuous multi-span beam in one direction and those of a single-span beam in the other direction in the Rayleigh-Ritz method to determine the eigenfrequencies of a thin orthotropic rectangular plate with uniform thickness. Xiang *et al*. (2002) studied the vibration behaviour of a ring supported cylindrically, based on the state-space technique and domain decomposition approach. Civalek *et al*. (2006, 2010) developed a discrete singular convolution algorithm to determine the frequencies for the free vibration of laminated conical shells and to study the buckling of rectangular Kirchhoff plates subjected to compressive loads on two-opposite edges. Lv *et al*. (2006) used the state-space approach in association with joint coupling matrices to analyze the free vibration of a rectangular Kirchhoff plate with two opposite simply-supported edges and internal line supports. Gürses (2009) used the discrete singular convolution method to investigate the free vibration of laminated skew plates. Rezaiguia and Laefer (2009) proposed a semi-analytical approach based on the modal method to determine the natural frequencies and mode shapes of a three-span continuous orthotropic rectangular plate with intermediate line rigid supports. Baltacıoglu *et al*. (2010) proposed a discrete singular convolution method to analyze the nonlinear static response of laminated composite plates. Talebitooti (2013) used the layerwise differential quadrature method to study the free vibration of

*Corresponding author, Postdoctor
E-mail: liangcao@cqu.edu.cn
[a]Professor

http://www.techno-press.com/journals/sem&subpage=7
ISSN: 1225-4568 (Print), 1598-6217 (Online)

thick, rotating laminated composite conical shells with different boundary conditions. Guebailia *et al*. (2013) proposed a local estimation method to calculate the fundamental frequencies and mode shapes of a three-span plate. Satouri *et al*. (2015) used the two-dimensional differential quadrature method (2D-DQM) to analyze the natural frequency of two-dimensional functionally graded material (2D-FGM) sectorial plate with variable thickness resting on elastic foundation.

This paper presents a new analytical approach to determine the natural frequencies and mode shapes of a multi-span continuous anisotropic plate with intermediate line rigid supports. The proposed approach is based on the combined modal and perturbation method, which considers the intermodal coupling effect. The implementation of this method is simple and gives accurate results in comparison with the published results.

2. Theoretical analysis on the vibration of anisotropic rectangular plates

2.1 Modeling assumptions

The following assumptions constitute the basis for solving the vibration problem of an anisotropic rectangular plate mathematically (Guebailia *et al*. 2013, Marchesiello *et al*. 1999, Zhu and Law 2002):

(1) Linear elastic behavior and negligible secondary effects (i.e., shearing and rotational inertia effects),

(2) Rigid intermediate supports and orthogonal free edges, and

(3) Thin plate.

Based on the above assumptions, the governing differential equation for a multi-span continuous anisotropic plate (a simplified model for long-span floors) of length L, width b, and uniform thickness h (Fig. 1) can be expressed by (Aoki and Maysenholder 2017, Zhou *et al*. 2017)

$$D_1\frac{\partial^4 W}{\partial x^4}+2D_3\frac{\partial^4 W}{\partial x^2\partial y^2}+D_2\frac{\partial^4 W}{\partial y^4}+c\frac{\partial W}{\partial t}+\frac{q_0}{g}\frac{\partial^2 W}{\partial t^2}=0 \tag{1}$$

where D_1 and D_2 are the plate stiffnesses in the x and y directions, respectively, D_3 is the sum of rigidities, g is the gravity acceleration, q_0 is the weight per unit area, c is the viscous damping coefficient, $W(x, y, t)$ is the deflection function, and t is the time variable.

In this study, a multi-span continuous plate with simply-supported condition on three edges ($x = 0$, $x = L$, $y = 0$, Fig. 1) and clamped condition on the remaining edge ($y = b$, Fig. 1) was considered.

2.2 Natural frequencies

Assuming the damping is negligible, the natural frequencies and mode shapes of the anisotropic rectangular plate can be determined by

$$D_1\frac{\partial^4 W}{\partial x^4}+2D_3\frac{\partial^4 W}{\partial x^2\partial y^2}+D_2\frac{\partial^4 W}{\partial y^4}+\frac{q_0}{g}\frac{\partial^2 W}{\partial t^2}=0 \tag{2}$$

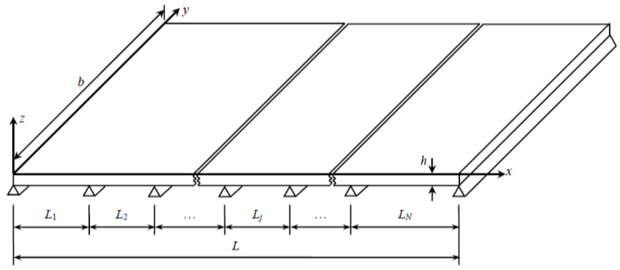

Fig. 1 Multi-span continuous anisotropic plate

When the plate vibrates in a natural mode, the vertical displacement $W(x, y, t)$ may be expressed as (Veletsos and Newmark 1956)

$$W(x,\ y,\ t)=\sum_{m=1}^{\infty}\sum_{n=1}^{\infty}u_{mn}\phi_{mn}(x,\ y)e^{-i\omega_{mn}t} \tag{3}$$

where ω_{mn} is the circular frequency, $\phi_{mn}(x,\ y)$ is the mode shape, u_{mn} is the modal amplitude, and $i = \sqrt{-1}$.

Substituting Eq. (3) into Eq. (2) results in

$$D_1\frac{\partial^4 \phi_{mn}}{\partial x^4}+2D_3\frac{\partial^4 \phi_{mn}}{\partial x^2\partial y^2}+D_2\frac{\partial^4 \phi_{mn}}{\partial y^4}-\omega_{mn}^2\frac{q_0}{g}\phi_{mn}=0 \tag{4}$$

The Rayleigh–Ritz method (Marchesiello *et al*. 1999, Jhung and Jeong 2015, Junior *et al*. 2017, Pradhan and Chakraverty 2015, Zhou 1994, Zhu and Law 2002) has been adopted by researchers to determine the natural frequencies and the mode shapes of an anisotropic rectangular plate, in which $\phi_{mn}(x,\ y)$ is decomposed as the product of two functions $X_m(x)$ and $Y_n(y)$ satisfying the boundary conditions in the x and y directions, respectively. The former is the eigenfunction of a multi-span continuous beam and the latter is the counterpart of a single-span beam. However, this decomposition neglects the intermodal coupling, thus resulting in slower convergence and higher computation cost (Guebailia *et al*. 2013, Rezaiguia and Laefer 2009).

To account for the intermodal coupling, $\phi_{mn}(x,\ y)$ can be treated as the product of the mode shape function for a multi-span continuous beam in x direction, $X_m(x)$, and the mode shape function $Y_{mn}(y)$ satisfying the boundary conditions of a plate in y direction, $Y_{mn}(y)$. Namely,

$$\phi_{mn}(x,\ y)=X_m(x)Y_{mn}(y) \tag{5}$$

$X_m(x)$ can be expressed by (See Appendix A for details)

$$X_m(x)=\begin{cases} A_{1m}\sin\alpha_m x+C_{1m}\sinh\alpha_m x & 0\le x\le L_1\\ \vdots & \vdots\\ A_{jm}\sin\alpha_m(x-\sum_{\zeta=1}^{j-1}L_\zeta)+B_{jm}\cos\alpha_m(x-\sum_{\zeta=1}^{j-1}L_\zeta)+C_{jm}\sinh\alpha_m(x-\sum_{\zeta=1}^{j-1}L_\zeta)+D_{jm}\cosh\alpha_m(x-\sum_{\zeta=1}^{j-1}L_\zeta) & \sum_{\zeta=1}^{j-1}L_\zeta\le x\le\sum_{\zeta=1}^{j}L_\zeta\\ \vdots & \vdots\\ A_{Nm}\sin\alpha_m(x-\sum_{\zeta=1}^{N-1}L_\zeta)+B_{Nm}\cos\alpha_m(x-\sum_{\zeta=1}^{N-1}L_\zeta)+C_{Nm}\sinh\alpha_m(x-\sum_{\zeta=1}^{N-1}L_\zeta)+D_{Nm}\cosh\alpha_m(x-\sum_{\zeta=1}^{N-1}L_\zeta) & \sum_{\zeta=1}^{N-1}L_\zeta\le x\le\sum_{\zeta=1}^{N}L_\zeta \end{cases} \tag{6}$$

The differentials in Eq. (4) must be satisfied for all x and y values. However, the solution for each value of x and y is practically impossible to be obtained. For this reason, it is suggested to substitute Eq. (5) into Eq. (3), multiply by $X_m(x)$, and then integrate the equation over the plate length along x direction. As such, one obtains

$$\frac{d^4Y_{mn}}{dy^4}+\frac{2D_3\theta_m}{D_2}\frac{d^2Y_{mn}}{dy^2}+\frac{gD_1\alpha_m^4-\omega_{mn}^2q_0}{gD_2}Y_{mn}=0 \tag{7}$$

where

$$\theta_m=\int_0^L\frac{d^2X_m}{dx^2}X_m dx\Big/\int_0^L X_m^2 dx \tag{8}$$

The boundary conditions in y direction are that the deflection and bending moment are zero, i.e.,

$$W(x,\ 0)=W(x,\ b)=0 \tag{9}$$

$$-D_2\left(\frac{\partial^2W}{\partial y^2}+\mu\frac{\partial^2W}{\partial x^2}\right)\bigg|_{y=0}=0,\quad \frac{\partial W}{\partial y}\bigg|_{y=b}=0 \tag{10}$$

Using Eqs. (3), (5), and (8), Eqs. (9) and (10) become

$$Y_{mn}(0)=Y_{mn}(b)=0 \tag{11}$$

$$\frac{d^2Y_{mn}}{dy^2}+\mu\theta_mY_{mn}\bigg|_{y=0}=0,\quad \frac{dY_{mn}}{dy}\bigg|_{y=b}=0 \tag{12}$$

The solution for Eq. (7) can be expressed by

$$\begin{aligned}Y_{mn}(y)&=\sin\beta_{mn}y+E_{mn}\cos\beta_{mn}y\\&+F_{mn}\sinh\gamma_{mn}y+G_{mn}\cosh\gamma_{mn}y\end{aligned} \tag{13}$$

$$\gamma_{mn}^2-\beta_{mn}^2=-2\frac{D_3}{D_2}\theta_m \tag{14}$$

where E_{mn}, F_{mn}, and G_{mn} are the constant coefficients determined by the boundary conditions (Eqs. (11) and (12), β_{mn} and γ_{mn} are the eigenvalues for the nth mode shape in the y direction.

Substituting Eq. (13) into the boundary conditions (Eqs. (11) and (12)) results in

$$\begin{bmatrix}0 & 1 & 0 & 1\\ 0 & \mu\theta_m-\beta_{mn}^2 & 0 & \mu\theta_m+\gamma_{mn}^2\\ \sin\beta_{mn}b & \cos\beta_{mn}b & \sinh\gamma_{mn}b & \cosh\gamma_{mn}b\\ \beta_{mn}\cos\beta_{mn}b & -\beta_{mn}\sin\beta_{mn}b & \gamma_{mn}\cosh\gamma_{mn}b & \gamma_{mn}\sinh\gamma_{mn}b\end{bmatrix}\begin{Bmatrix}1\\E_{mn}\\F_{mn}\\G_{mn}\end{Bmatrix}=\begin{Bmatrix}0\\0\\0\\0\end{Bmatrix} \tag{15}$$

For a non-trivial solution of Eq. (15), the following equation must be satisfied

$$\gamma_{mn}\cosh\gamma_{mn}b\sin\beta_{mn}b-\beta_{mn}\cos\beta_{mn}b\sinh\gamma_{mn}b=0 \tag{16}$$

where the parameters β_{mn} and γ_{mn} can be solved using the perturbation method (See Section 2.3) and the circular frequency ω_{mn} can be obtained from the following expression

$$\omega_{mn}=\sqrt{\frac{g(D_1\alpha_m^4+D_2\beta_{mn}^2\gamma_{mn}^2)}{q_0}} \tag{17}$$

The expressions for the constant coefficients E_{mn}, F_{mn}, and G_{mn} are

$$E_{mn}=G_{mn}=0,\quad F_{mn}=-\sin\beta_{mn}b\,\mathrm{csch}\gamma_{mn}b \tag{18}$$

Lastly, the mode shapes of the anisotropic rectangular thin plate are represented by

$$\begin{aligned}\phi_{mn}(x,\ y)&=X_m(x)Y_{mn}(y)\\&=X_m(x)(\sin\beta_{mn}y-\sin\beta_{mn}b\,\mathrm{csch}\gamma_{mn}b\sinh\gamma_{mn}y)\end{aligned} \tag{19}$$

2.3 Perturbation solution for coefficients β_{mn} and γ_{mn}

To solve Eqs. (14) and (16), the perturbation method (Karahan and Pakdemirli 2017, Poloei *et al*. 2017) was adopted in this study along with the condition, $D_2 > D_3$. Letting $\varepsilon = D_3/D_2$, Eq. (14) becomes

$$\gamma_{mn}^2-\beta_{mn}^2=-2\varepsilon\theta_m \tag{20}$$

Since coefficient $\varepsilon < 1$ generally, it was chosen as the perturbation parameter. Thus, parameters β_{mn} and γ_{mn} can be expanded with respect to ε as follows

$$\begin{aligned}\beta_{mn}&=\beta_{mn0}+\varepsilon\beta_{mn1}+\varepsilon^2\beta_{mn2}+\varepsilon^3\beta_{mn3}+\cdots\\&+\varepsilon^k\beta_{mnk}+\cdots=\sum_{k=0}^{\infty}\varepsilon^k\beta_{mnk}\end{aligned} \tag{21}$$

$$\begin{aligned}\gamma_{mn}&=\gamma_{mn0}+\varepsilon\gamma_{mn1}+\varepsilon^2\gamma_{mn2}+\varepsilon^3\gamma_{mn3}+\cdots\\&+\varepsilon^k\gamma_{mnk}+\cdots=\sum_{k=0}^{\infty}\varepsilon^k\gamma_{mnk}\end{aligned} \tag{22}$$

First, substituting Eqs. (21) and (22) into Eqs. (16) and (20) and equating the terms of order ε^0 gives the following equations (See Appendix B for details)

$$\gamma_{mn0}^2-\beta_{mn0}^2=0 \tag{23}$$

$$\gamma_{mn0}\cosh\gamma_{mn0}b\sin\beta_{mn0}b-\beta_{mn0}\cos\beta_{mn0}b\sinh\gamma_{mn0}b=0 \tag{24}$$

which give the first approximate solution as

$$\beta_{mn0}=\gamma_{mn0}\approx\frac{(4n+1)\pi}{4b} \tag{25}$$

Next, equating the terms of order ε yields the following equations

$$\frac{(4n+1)\pi}{4b}(\gamma_{mn1}-\beta_{mn1})+\theta_m=0 \tag{26}$$

$$\begin{aligned}&e^{\frac{(4n+1)\pi}{4}}\{[(4n+1)\pi-2]\beta_{mn1}+2\gamma_{mn1}\}\\&+e^{-\frac{(4n+1)\pi}{4}}\{2\beta_{mn1}-[(4n+1)\pi-2]\gamma_{mn1}\}=0\end{aligned} \tag{27}$$

which give the second approximations as

$$\beta_{mn1}=\frac{4b[2e^{\frac{(4n+1)\pi}{2}}-(4n+1)\pi+2]\theta_m}{(4n+1)\pi\{4+[e^{\frac{(4n+1)\pi}{2}}-1](4n+1)\pi\}} \tag{28}$$

$$\gamma_{mn1}=-\frac{4b\{[(4n+1)\pi-2]e^{\frac{(4n+1)\pi}{2}}+2\}\theta_m}{(4n+1)\pi\{4+[e^{\frac{(4n+1)\pi}{2}}-1](4n+1)\pi\}} \tag{29}$$

Table 1 The geometry of a multi-span

N-span	L_1 (m)	L_2 (m)	L_3 (m)	L_4 (m)
1	24	---	---	---
2	24	24	---	---
3	24	30	24	---
4	24	30	32	24

(Note: L_j is the length of the jth span plate)

Likewise, for the third approximation, equating the terms of order ε^2 yields the following equations

$$\begin{aligned}&[(4n+1)\pi-4](4n+1)^3\pi^3(\beta_{mn2}-\gamma_{mn2})\\&+32(4n+1)\pi b^3\theta_m^2+e^{\frac{(4n+1)\pi}{2}}\{32[(4n+1)\pi-4]b^3\theta_m^2\\&-(4n+1)^4\pi^4(\beta_{mn2}-\gamma_{mn2})\}=0\end{aligned}\tag{30}$$

$$\begin{aligned}&(4n+1)^2\pi^2[(4n+1)\pi-4]^2\{2\beta_{mn2}-[(4n+1)\pi-2]\gamma_{mn2}\}-8b^3[32-16(4n+1)\pi\\&+(4n+1)^3\pi^3]\theta_m^2+e^{\frac{(4n+1)\pi}{2}}[(4n+1)^5\pi^5(\beta_{mn2}+2\gamma_{mn2})-2(4n+1)^4\pi^4(7\beta_{mn2}+5\gamma_{mn2})\\&+48(4n+1)^3\pi^3\beta_{mn2}+256b^3\theta_m^2-320(4n+1)\pi b^3\theta_m^2-32(4n+1)^2\pi^2(\beta_{mn2}-\gamma_{mn2}\\&-4b^3\theta_m^2)]-e^{(4n+1)\pi}[(4n+1)^5\pi^5(2\beta_{mn2}+\gamma_{mn2})-2(4n+1)^4\pi^4(7\beta_{mn2}-\gamma_{mn2})\\&+256b^3\theta_m^2-128(4n+1)\pi b^3\theta_m^2+128(4n+1)^2\pi^2b^3\theta_m^2+8(4n+1)^3\pi^3(2\beta_{mn2}-2\gamma_{mn2}\\&-3b^3\theta_m^2)]+e^{\frac{3(4n+1)\pi}{2}}\{(4n+1)^4\pi^4\{[(4n+1)\pi-2]\beta_{mn2}+2\gamma_{mn2}\}-64b^3[(4n+1)\pi\\&-4]\theta_m^2\}=0\end{aligned}\tag{31}$$

which give the following solutions

$$\begin{aligned}\beta_{mn2}=&\frac{8b^3\theta_m^2}{(4n+1)^3\pi^3\{4+[e^{\frac{(4n+1)\pi}{2}}-1](4n+1)\pi\}^3}\{(4n+1)\pi\{64+(4n+1)\pi\{-40\\&+(4n+1)\pi[(4n+1)\pi+4]\}\}-16e^{\frac{(4n+1)\pi}{2}}[8-8(4n+1)\pi+(4n+1)^3\pi^3]\\&+e^{(4n+1)\pi}\{-128+(4n+1)\pi\{64+(4n+1)\pi\{8-3(4n+1)\pi[(4n+1)\pi-4]\}\}\}\\&+16e^{\frac{3(4n+1)\pi}{2}}(4n+1)\pi[(4n+1)\pi-4]\}\end{aligned}\tag{32}$$

$$\begin{aligned}\gamma_{mn2}=&-\frac{8b^3\theta_m^2}{(4n+1)^3\pi^3\{4+[e^{\frac{(4n+1)\pi}{2}}-1](4n+1)\pi\}^3}\{(4n+1)^2\pi^2[8-(4n+1)^2\pi^2]\\&+4e^{\frac{(4n+1)\pi}{2}}\{-32+(4n+1)\pi\{16+(4n+1)\pi[3(4n+1)\pi-4]\}\}+e^{(4n+1)\pi}\{128\\&+(4n+1)\pi\{-192+(4n+1)\pi\{56+(4n+1)\pi[3(4n+1)\pi-16]\}\}\}\\&+4e^{\frac{3(4n+1)\pi}{2}}(4n+1)\pi[(4n+1)\pi-4]^2\}\end{aligned}\tag{33}$$

The computation may be ended at this point depending on the required precision.

3. Modal Parameters analysis

3.1 Validation of coefficients β_{mn} and γ_{mn}

In order to verify the perturbation solution of coefficients β_{mn} and γ_{mn}, an example analysis is presented here. The geometry of a multi-span continuities anisotropic rectangular prestressed concrete plate (Cao *et al*. 2018) is indicated in Table 1, where the coefficients E (Young's modulus), D_1, D_2, D_3, q_0, b, and μ_p (Poisson's ratio) are respectively 3.25×10^{10} Pa, 4.08×10^8 N·m, 4.44×10^8 N·m, 4.88×10^6 N·m, 7165.13 N/m^2, 24 m, and 0.2. The β_{mn} and γ_{mn} coefficients calculated by the perturbation and numerical methods are listed in Tables 2 and 3, respectively. As seen from the tables, the maximum difference between the two methods is merely 3.68×10^{-2}% for coefficient β_{mn} and 6.67×10^{-2}% for coefficient γ_{mn}, thus validating the perturbation method.

Table 2 Computed β_{mn} coefficients

N-span			m = 1	2	3	4	5
1	β_{m1}	Perturbation method	0.163479	0.163052	0.162370	0.161479	0.160442
		Numerical method	0.163463	0.163037	0.162355	0.161454	0.160383
		Error ($\times10^{-2}$%)	0.98	0.92	0.92	1.55	**3.68**
	β_{m2}	Perturbation method	0.294479	0.294345	0.294124	0.293822	0.293446
		Numerical method	0.294479	0.294345	0.294124	0.293822	0.293444
		Error ($\times10^{-2}$%)	0.00	0.00	0.00	0.00	0.07
	β_{m3}	Perturbation method	0.425402	0.425338	0.425231	0.425082	0.424895
		Numerical method	0.425402	0.425338	0.425231	0.425082	0.424894
		Error ($\times10^{-2}$%)	0.00	0.00	0.00	0.00	0.02
2	β_{m1}	Perturbation method	0.163479	0.163455	0.163052	0.163003	0.162370
		Numerical method	0.163463	0.163439	0.163037	0.162989	0.162355
		Error ($\times10^{-2}$%)	0.98	0.98	0.92	0.86	0.92
	β_{m2}	Perturbation method	0.294479	0.294472	0.294345	0.294329	0.294124
		Numerical method	0.294479	0.294472	0.294345	0.294329	0.294124
		Error (%)	0.00	0.00	0.00	0.00	0.00
	β_{m3}	Perturbation method	0.425402	0.425399	0.425338	0.425330	0.425231
		Numerical method	0.425402	0.425399	0.425338	0.425330	0.425231
		Error (%)	0.00	0.00	0.00	0.00	0.00
3	β_{m1}	Perturbation method	0.163513	0.163466	0.163473	0.163215	0.163026
		Numerical method	0.163497	0.163450	0.163458	0.16320	0.163011
		Error ($\times10^{-2}$%)	0.98	0.98	0.92	0.92	0.92
	β_{m2}	Perturbation method	0.294490	0.294475	0.294477	0.294396	0.294336
		Numerical method	0.294490	0.294475	0.294477	0.294396	0.294336
		Error (%)	0.00	0.00	0.00	0.00	0.00
	β_{m3}	Perturbation method	0.425407	0.425400	0.425401	0.425363	0.425334
		Numerical method	0.425407	0.425400	0.425401	0.425363	0.425334
		Error (%)	0.00	0.00	0.00	0.00	0.00
4	β_{m1}	Perturbation method	0.163530	0.163505	0.163467	0.163480	0.163273
		Numerical method	0.163514	0.163489	0.163451	0.163464	0.163257
		Error ($\times10^{-2}$%)	0.98	0.98	0.98	0.98	0.98
	β_{m2}	Perturbation method	0.294495	0.294487	0.294475	0.294479	0.294415
		Numerical method	0.294495	0.294487	0.294475	0.294479	0.294414
		Error ($\times10^{-2}$%)	0.00	0.00	0.00	0.00	0.03
	β_{m3}	Perturbation method	0.425410	0.425406	0.425401	0.425402	0.425371
		Numerical method	0.425410	0.425406	0.425401	0.425402	0.425371
		Error (%)	0.00	0.00	0.00	0.00	0.00

3.2 Comparison of natural frequencies

The calculated natural frequencies for the N-span continuous plate (N = 1, 2, 3, 4) with and without

Table 3 Computed γ_{mn} coefficients

N-span			m				
			1	2	3	4	5
1	γ_{m1}	Perturbation method	0.164627	0.167607	0.172484	0.179121	0.187329
		Numerical method	0.164611	0.167594	0.172479	0.179148	0.187454
		Error ($\times10^{-2}$%)	0.97	0.78	0.29	1.50	**6.67**
	γ_{m2}	Perturbation method	0.295118	0.296893	0.299831	0.303901	0.309060
		Numerical method	0.295118	0.296863	0.299831	0.303904	0.309072
		Error ($\times10^{-2}$%)	0.00	1.01	0.00	0.10	0.39
	γ_{m3}	Perturbation method	0.425845	0.427105	0.429198	0.432112	0.435832
		Numerical method	0.425845	0.427105	0.429198	0.432113	0.435834
		Error ($\times10^{-2}$%)	0.00	0.00	0.00	0.02	0.05
2	γ_{m1}	Perturbation method	0.164627	0.164794	0.167607	0.167949	0.172484
		Numerical method	0.164611	0.164778	0.167594	0.167936	0.172479
		Error ($\times10^{-2}$%)	0.97	0.97	0.78	0.77	0.29
	γ_{m2}	Perturbation method	0.295118	0.295217	0.296893	0.297097	0.299831
		Numerical method	0.295118	0.295217	0.296893	0.297097	0.299831
		Error (%)	0.00	0.00	0.00	0.00	0.00
	γ_{m3}	Perturbation method	0.425845	0.425915	0.427105	0.427250	0.429198
		Numerical method	0.425845	0.425915	0.427105	0.427250	0.429198
		Error (%)	0.00	0.00	0.00	0.00	0.00
3	γ_{m1}	Perturbation method	0.164392	0.164719	0.164668	0.166461	0.167793
		Numerical method	0.164376	0.164704	0.164652	0.166447	0.167779
		Error ($\times10^{-2}$%)	0.97	0.91	0.97	0.84	0.83
	γ_{m2}	Perturbation method	0.294479	0.295173	0.295142	0.296209	0.297004
		Numerical method	0.294479	0.295173	0.295142	0.296209	0.297004
		Error (%)	0.00	0.00	0.00	0.00	0.00
	γ_{m3}	Perturbation method	0.425746	0.425884	0.425862	0.426619	0.427184
		Numerical method	0.425746	0.425884	0.425862	0.426619	0.427184
		Error (%)	0.00	0.00	0.00	0.00	0.00
4	γ_{m1}	Perturbation method	0.164277	0.164451	0.164711	0.164620	0.166061
		Numerical method	0.164261	0.164435	0.164695	0.164605	0.166047
		Error ($\times10^{-2}$%)	0.97	0.97	0.97	0.91	0.84
	γ_{m2}	Perturbation method	0.294911	0.295013	0.295168	0.295114	0.295970
		Numerical method	0.294911	0.295013	0.295167	0.295114	0.295970
		Error ($\times10^{-2}$%)	0.00	0.00	0.03	0.00	0.00
	γ_{m3}	Perturbation method	0.425698	0.425771	0.425880	0.425842	0.426450
		Numerical method	0.425698	0.425771	0.425880	0.425842	0.426450
		Error (%)	0.00	0.00	0.00	0.00	0.00

considering the intermodal coupling are listed in Table 4. The first four mode shapes of the 3-span continuous anisotropic rectangular plate are shown in Fig. 2. As indicated in Table 4, the maximum difference for the natural frequencies is 5.12% between the case considering the intermodal coupling and that without considering it.

To compare the high frequencies of multi-span plates, Table 5 lists the first six frequencies of a three-span continues anisotropic rectangular plate with the span lengths of 10 m, 12 m, and 10 m. Table 5 demonstrates that the relative errors between the case with the intermodal coupling and that without it are negligible and hence the intermodal coupling effect may be ignored.

Table 4 Comparison of the natural frequencies of the anisotropic plate obtained by different methods

N-span	Intermodal coupling	The *k*th natural frequency					
		1	2	3	4	5	6
1	Included (Hz)	3.91	8.83	10.97	13.56	18.66	21.35
	Excluded (Hz)	4.11	8.80	11.09	13.50	18.77	21.47
	Error (%)	**5.12**	0.34	1.09	0.44	0.59	0.56
2	Included (Hz)	3.91	4.61	8.82	10.86	10.97	11.24
	Excluded (Hz)	3.89	4.72	8.8	10.5	10.92	11.31
	Error (%)	0.51	2.39	0.23	3.31	0.46	0.62
3	Included (Hz)	3.71	4.18	4.55	7.16	9.52	10.90
	Excluded (Hz)	3.74	4.17	4.62	7.13	9.58	10.50
	Error (%)	0.81	0.24	1.54	0.42	0.63	3.67
4	Included (Hz)	3.62	3.87	4.29	4.48	6.39	7.55
	Excluded (Hz)	3.61	3.91	4.26	4.54	6.36	7.55
	Error (%)	0.28	1.03	0.70	1.34	0.47	0.00

Table 5 Natural frequencies for the high frequencies of a three-span continues plate

Intermodal coupling	The *k*th natural frequency					
	1	2	3	4	5	6
Included (Hz)	10.54	14.74	15.01	18.22	18.70	21.36
Excluded (Hz)	10.60	14.78	14.96	18.14	18.78	21.46
Error (%)	**0.57**	0.27	0.33	0.44	0.43	0.47

4. Conclusions

In this paper, the function defining the mode shapes of a multi-span continuous anisotropic plate is treated as the product of two admissible functions. One defines the longitudinal mode shapes of the plate as those corresponding to a multi-span continuous beam with simply-supported edges. The other defines the transverse mode shapes of a single-span beam with the intermodal coupling effect which has been often omitted to avoid the complicated calculation. This decomposition converts the boundary conditions into a differential equation that requires a complex solution process. To ease the solving process, the perturbation method was developed to calculate the natural frequencies of the multi-span continuous anisotropic plate. Compared to the more accurate numerical results, the maximum relative error resulting from the perturbation method is merely 3.68×10^{-2}% for coefficient β_{mn} (Eq. (21)) and 6.67×10^{-2}% for coefficient γ_{mn} (Eq. (22)), thus validating the perturbation method. The maximum difference of the natural frequencies for the *N*-span continuous plate (N = 1, 2, 3, 4) is noticeable at 5.12% between the case with the intermodal coupling and that

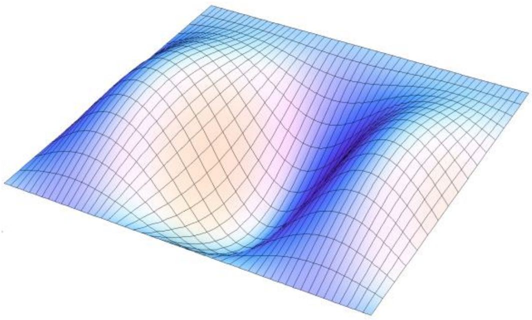

(a) First mode shape

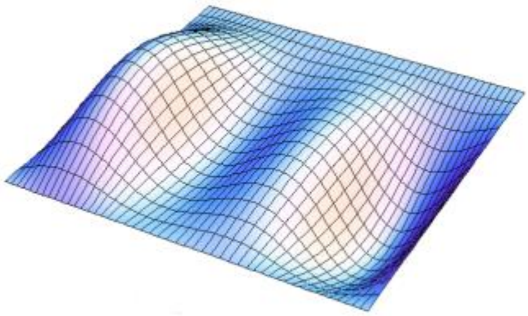

(b) Second mode shape

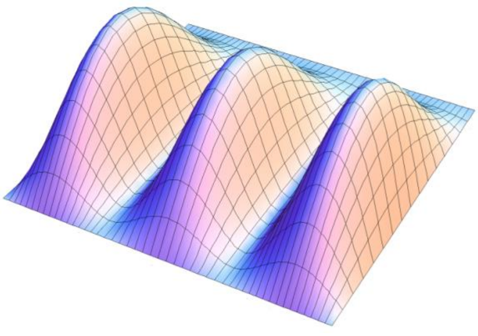

(c) Third mode shape

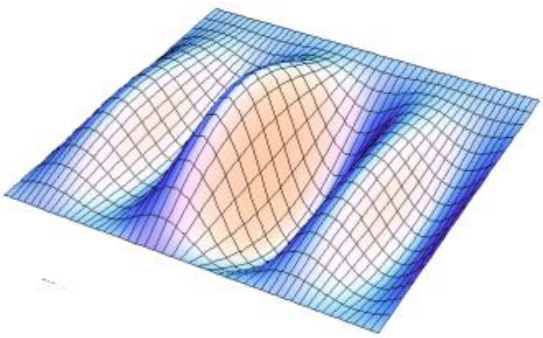

(d) Fourth mode shape

Fig. 2 The first four mode shapes of the 3-span continuous plate (intermodal coupling included)

without it. For the high frequencies of multi-span plates, the difference between these two cases is small, however, therefore the intermodal coupling effect may be ignored.

Acknowledgments

The authors are grateful for the financial support provided by the National Natural Science Foundation of China (Grant No. 51622802, 51438001) and Chongqing Basic and Frontier Research Project (Grant No. cstc2014jcyjys30001).

References

Aoki, Y. and Maysenholder, W. (2017), "Experimental and numerical assessment of the equivalent-orthotropic-thin-plate model for bending of corrugated panels", *Int. J. Solids Struct.*, **108**, 11-23.

Azimi, S., Hamilton, J.F. and Soedel, W. (1984), "The receptance method applied to the free vibration of continuous rectangular plates", *J. Sound Vib.*, **93**(l), 9-29.

Baltacıoglu, A.K., Akgoz, B. and Civalek, O. (2010), "Nonlinear static response of laminated composite plates by discrete singular convolution method", *Compos. Struct.*, **93**(1), 153-161.

Cao, L., Liu, J.P., Li, J. and Zhang, R.Z. (2018), "Experimental and analytical studies on the vibration serviceability of long-span prestressed concrete floor", *Earthq. Eng. Eng. Vibr.*, **17**(2), 417-428.

Chen, J., Peng, Y. and Ye, T. (2013), "On methods for extending a single footfall trace into a continuous force curve for floor vibration serviceability analysis", *Struct. Eng. Mech.*, **46**(2), 179-196.

Civalek, O. (2006), "The determination of frequencies of laminated conical shells via the discrete singular convolution method", *J. Mech. Mater. Struct.*, **1**(1), 163-182.

Civalek, O., Korkmaz, A. and Demir, C. (2010), "Discrete singular convolution approach for buckling analysis of rectangular Kirchhoff plates subjected to compressive loads on two-opposite edges", *Adv. Eng. Softw.*, **41**(4), 557-560.

De Matos Junior, O.D., Donadon, M.V. and Castro, S.G.P. (2017), "Aeroelastic behavior of stiffened composite laminated panel with embedded SMA wire using the hierarchical Rayleigh-Ritz method", *Compos. Struct.*, **181**, 26-45.

Dickinson, S.M. and Warburton, G.B. (1967), "Natural frequencies of plate systems using the edge-effect method", *J. Mech. Eng. Sci.*, **9**(4), 318-324.

Elishakoff, I. and Sternberg, A. (1979), "Eigenfrequencies of continuous plates with arbitrary number of equal spans", *J. Appl. Mech.*, **46**(3), 656-662.

Gorman, D.J. and Garibaldi, L. (2006), "Accurate analytical type solutions for free vibration frequencies and mode shapes of multi-span bridge decks: the span-by-span approach", *J. Sound Vib.*, **290**(1), 321-336.

Guebailia, M., Ouelaa, N. and Guyader, J.L. (2013), "Solution of the free vibration equation of a multi span bridge deck by local estimation method", *Eng. Struct.*, **48**, 695-703.

Gürses, M., Civalek, O., Korkmaz, A. and Ersoy, H. (2009), "Free vibration analysis of symmetric laminated skew plates by discrete singular convolution technique based on first-order shear deformation theory", *Int. J. Numer. Meth. Eng.*, **79**(3), 290-313.

Jhung, M.J. and Jeong, K.H. (2015), "Modal characteristics of partially perforated rectangular plate with triangular penetration pattern", *Struct. Eng. Mech.*, **55**(3), 583-603.

Karahan, M.M.F. and Pakdemirli, M. (2017). "Vibration analysis of a beam on a nonlinear elastic foundation", *Struct. Eng. Mech.*, **62**(2), 171-178.

Lin, Y.K., Brown, I.D. and Deutschle, P.C. (1964), "Free vibrations of a finite row of continuous skin-stringer panels", *J. Sound Vib.*, **1**(1), 14-27.

Lü, C.F., Lee, Y.Y., Lim, C.W. and Chen, W.Q. (2006), "Free vibration of long-span continuous rectangular Kirchhoff plates with internal rigid line supports", *J. Sound Vibr.*, **297**(1-2), 351-

364.

Marchesiello, S., Fasana, A., Garibaldi, L. and Piombo, B.A.D. (1999), "Dynamics of multi-span continuous straight bridges subject to multi-degrees of freedom moving vehicle excitation", *J. Sound Vibr.*, **224**(3), 541-61.

Mercer, C.A. and Seavey, M.C. (1967), "Prediction of natural frequencies and normal modes of skin-stringer panel rows", *J. Sound Vibr.*, **6**(1), 149-162.

Poloei, E., Zamanian, M. and Hosseini, S.A.A. (2017), "Nonlinear vibration analysis of an electrostatically excited micro cantilever beam coated by viscoelastic layer with the aim of finding the modified configuration", *Struct. Eng. Mech.*, **61**(2), 193-207.

Pradhan, K.K. and Chakraverty, S. (2015), "Free vibration of functionally graded thin elliptic plates with various edge supports", *Struct. Eng. Mech.*, **53**(2), 337-354.

Rezaiguia, A. and Laefer, D.F. (2009), "Semi-analytical determination of natural frequencies and mode shapes of multi-span bridge decks", *J. Sound Vibr.*, **328**(13), 291-300.

Satouri, S., Asanjarani, A. and Satouri, A. (2015), "Natural frequency analysis of 2D-FGM sectorial plate with variable thickness resting on elastic foundation using 2D-DQM", *Int. J. Appl. Mech.*, **7**(2), 1550030.

Talebitooti, M. (2013), "Three-dimensional free vibration analysis of rotating laminated conical shells: layerwise differential quadrature (LW-DQ) method", *Arch. Appl. Mech.*, **83**(5), 765-781.

Ungar. E.E. (1960), "Free oscillations of edge-connected simply supported plate systems", *J. Eng. Ind.*, **83**(4), 434-439.

Veletsos, A.S. and Newmark, N.M. (1956), "Determination of natural frequencies of continuous plates hinged along two edges", *J. Appl. Mech.*, **23**(1), 97-102.

Wang, J.P. and Chen, J. (2017), "A comparative study on different walking load models", *Struct. Eng. Mech.*, **63**(6), 847-856.

Xiang, Y., Ma, Y.F., Kitiornchai, S., Lim, C.W. and Lau, C.W.H. (2002), "Exact solutions for vibration of cylindrical shells with intermediate ring supports", *Int. J. Mech. Sci.*, **44**, 1907-24.

Zhou, D. (1994), "Eigenfrequencies of line supported rectangular plates", *Int. J. Solids Struct.*, **31**(3), 347-358.

Zhou, X.H., Liu, J.P., Cao, L. and Li, J. (2017), "Vibration serviceability of pre-stressed concrete floor system under human activity", *Struct. Infrastruct. E.*, **13**(8), 967-977.

Zhu, X.Q. and Law, S.S. (2002), "Dynamic load on continuous multi-lane bridge deck from moving vehicles", *J. Sound Vibr.*, **251**(4), 697-716.

PL

Appendix A: Mode shapes of a multi-span continuous beam with simply supported edges

To identify the natural mode shapes of a multi-span continuous beam with simply-supported edges (Fig. A.1), it is necessary to know the natural mode shapes in each span considering the boundary and continuity conditions. Assuming same bending stiffness for each span, the formulation of *m*th mode shape for the *j*th span is

$$\begin{aligned} X_{jm}(x_j) &= A_{jm}\sin\alpha_m x_j + B_{jm}\cos\alpha_m x_j \\ &+C_{jm}\sinh\alpha_m x_j + D_{jm}\cosh\alpha_m x_j \end{aligned} \tag{A.1}$$

where Ajm, Bjm, Cjm, and Djm are the coefficients determined by the boundary and continuity conditions and αm is the eigenvalue for the mth mode shape of the multi-span beam.

The boundary conditions are described as follows

$$X_{jm}(x_j)\big|_{x_j=0} = X_{jm}(x_j)\big|_{x_j=L_j} = 0 \quad j=1,\ 2,\ 3,\ \cdots,\ N \tag{A.2}$$

$$\left.\frac{d^2X_{1m}}{dx_1^2}\right|_{x_1=0} = \left.\frac{d^2X_{Nm}}{dx_N^2}\right|_{x_N=L_N} = 0 \tag{A.3}$$

The continuity conditions for the intermediate supports are as such

$$\left.\begin{aligned} \left.\frac{dX_{jm}}{dx_j}\right|_{x_j=L_j} &= \left.\frac{dX_{(j+1)m}}{dx_{j+1}}\right|_{x_{j+1}=0} \\ \left.\frac{d^2X_{jm}}{dx_j^2}\right|_{x_j=L_j} &= \left.\frac{d^2X_{(j+1)m}}{dx_{j+1}^2}\right|_{x_{j+1}=0} \end{aligned}\right. \quad j=1,\ 2,\ 3,\ \cdots,\ N-1 \tag{A.4}$$

Substituting Eq. (A.1) into the boundary conditions (Eqs. (A.2) and (A.3)) and continuity conditions (Eq. (A.4)) results in

$$C_{1m} = -A_{1m}\frac{\sin\alpha_m L_1}{\sinh\alpha_m L_1},\quad B_{1m} = D_{1m} = 0 \tag{A.5}$$

$$\begin{aligned} A_{(j+1)m} &= \frac{1}{\sin\alpha_m L_{j+1} - \sinh\alpha_m L_{j+1}}\left[-\frac{\sinh\alpha_m L_{j+1}}{\alpha_m}\frac{dX_{jm}(x_j)}{dx_j}\right. \\ &\left.\left.+\frac{\cos\alpha_m L_{j+1} - \cosh\alpha_m L_{j+1}}{2\alpha_m^2}\frac{d^2X_{jm}(x_j)}{dx_j^2}\right]\right|_{x_j=L_j} \end{aligned} \tag{A.6}$$

$$B_{(j+1)m} = -\frac{1}{2\alpha_m^2}\left.\frac{d^2X_{jm}(x_j)}{dx_j^2}\right|_{x_j=L_j} \tag{A.7}$$

$$\begin{aligned} C_{(j+1)m} &= \frac{1}{\sin\alpha_m L_{j+1} - \sinh\alpha_m L_{j+1}}\left[\frac{\sin\alpha_m L_{j+1}}{\alpha_m}\frac{dX_{jm}(x_j)}{dx_j}\right. \\ &\left.\left.+\frac{\cosh\alpha_m L_{j+1} - \cos\alpha_m L_{j+1}}{2\alpha_m^2}\frac{d^2X_{jm}(x_j)}{dx_j^2}\right]\right|_{x_j=L_j} \end{aligned} \tag{A.8}$$

$$D_{(j+1)m} = \frac{1}{2\alpha_m^2}\left.\frac{d^2X_{jm}(x_j)}{dx_j^2}\right|_{x_j=L_j} \tag{A.9}$$

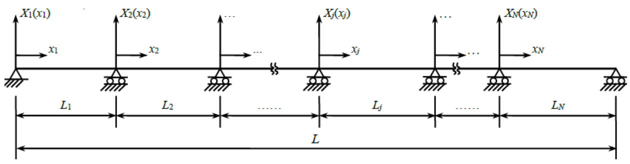

Fig. A.1 Multi-span continuous beam with simply-supported edges

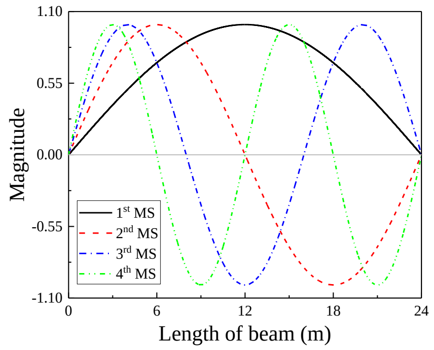

(a) $N = 1$ ($L_1 = 24$ m)

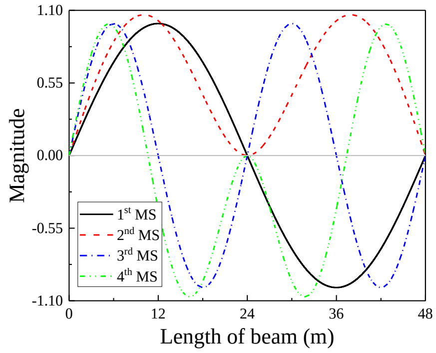

(b) $N = 2$ ($L_1 = L_2 = 24$ m)

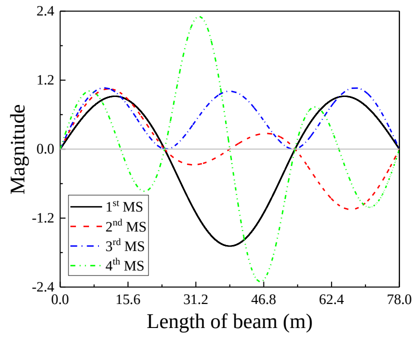

(c) $N = 3$ ($L_1 = L_3 = 24$ m, $L_2 = 30$ m)

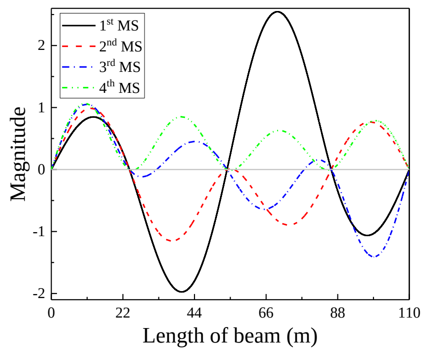

(d) $N = 4$ ($L_1 = L_4 = 24$ m, $L_2 = 30$ m, $L_3 = 32$ m)

Fig. A.2 The first four mode shapes of a N-span beam (N = 1, 2, 3, 4)

where j = 1, 2, 3, …, N-1.

The eigenvalue α_m for the mth mode shape of the multi-span beam is determined by

$$\begin{aligned} &-A_{Nm}\sin\alpha_m L_N - B_{Nm}\cos\alpha_m L_N \\ &+C_{Nm}\sinh\alpha_m L_N + D_{Nm}\cosh\alpha_m L_N = 0 \end{aligned} \tag{A.10}$$

Then, the expression for the mth mode shape of the multi-span beam can be written as

$$X_m(x) = \begin{cases} A_{1m}\sin\alpha_m x + C_{1m}\sinh\alpha_m x & 0 \le x \le L_1 \\ \vdots & \vdots \\ A_{jm}\sin\alpha_m(x-\sum_{\zeta=1}^{j-1}L_\zeta) + B_{jm}\cos\alpha_m(x-\sum_{\zeta=1}^{j-1}L_\zeta) + C_{jm}\sinh\alpha_m(x-\sum_{\zeta=1}^{j-1}L_\zeta) + D_{jm}\cosh\alpha_m(x-\sum_{\zeta=1}^{j-1}L_\zeta) & \sum_{\zeta=1}^{j-1}L_\zeta \le x \le \sum_{\zeta=1}^{j}L_\zeta \\ \vdots & \vdots \\ A_{Nm}\sin\alpha_m(x-\sum_{\zeta=1}^{N-1}L_\zeta) + B_{Nm}\cos\alpha_m(x-\sum_{\zeta=1}^{N-1}L_\zeta) + C_{Nm}\sinh\alpha_m(x-\sum_{\zeta=1}^{N-1}L_\zeta) + D_{Nm}\cosh\alpha_m(x-\sum_{\zeta=1}^{N-1}L_\zeta) & \sum_{\zeta=1}^{N-1}L_\zeta \le x \le \sum_{\zeta=1}^{N}L_\zeta \end{cases} \tag{A.11}$$

According to Eq. (A.11) , the first four mode shapes of a N-span beam (N = 1, 2, 3, 4) with different spans are shown in Fig. A.2.

(Note: MS = mode shape)

Appendix B: Asymptotic function of elementary function

For the trigonometric and exponential functions, the asymptotic functions are expressed by

$$\begin{aligned}&\sin(\xi_0+\varepsilon\xi_1+\varepsilon^2\xi_2+\varepsilon^3\xi_3+\varepsilon^4\xi_4)\\&=\sin\xi_0+\varepsilon\xi_1\cos\xi_0+\varepsilon^2(\xi_2\cos\xi_0-\frac{1}{2}\xi_1^2\sin\xi_0)\\&+\varepsilon^3[(\xi_3-\frac{1}{6}\xi_1^3)\cos\xi_0-\xi_1\xi_2\sin\xi_0]+\varepsilon^4[(\xi_4-\frac{1}{2}\xi_1^2\xi_2)\cos\xi_0\\&+\frac{1}{24}(\xi_1^4-12\xi_2^2-24\xi_1\xi_3)\sin\xi_0]+O(\varepsilon^5)\end{aligned} \tag{B.1}$$

$$\begin{aligned}&\cos(\xi_0+\varepsilon\xi_1+\varepsilon^2\xi_2+\varepsilon^3\xi_3+\varepsilon^4\xi_4)\\&=\cos\xi_0-\varepsilon\xi_1\sin\xi_0-\varepsilon^2(\xi_2\sin\xi_0+\frac{1}{2}\xi_1^2\cos\xi_0)\\&+\varepsilon^3[(\frac{1}{6}\xi_1^3-\xi_3)\sin\xi_0-\xi_1\xi_2\cos\xi_0]+\varepsilon^4[(\frac{1}{2}\xi_1^2\xi_2-\xi_4)\sin\xi_0\\&+\frac{1}{24}(\xi_1^4-12\xi_2^2-24\xi_1\xi_3)\cos\xi_0]+O(\varepsilon^5)\end{aligned} \tag{B.2}$$

$$\begin{aligned}&e^{\xi_0+\varepsilon\xi_1+\varepsilon^2\xi_2+\varepsilon^3\xi_3+\varepsilon^4\xi_4}=e^{\xi_0}+\varepsilon\xi_1e^{\xi_0}+\frac{1}{2}\varepsilon^2(\xi_1^2+2\xi_2)e^{\xi_0}\\&+\frac{1}{6}\varepsilon^3(\xi_1^3+6\xi_1\xi_2+6\xi_3)e^{\xi_0}+\frac{1}{24}\varepsilon^4(\xi_1^4+12\xi_1^2\xi_2\\&+24\xi_1\xi_3+12\xi_2^2+24\xi_4)e^{\xi_0}+O(\varepsilon^5)\end{aligned} \tag{B.3}$$

$$\begin{aligned}&e^{-(\xi_0+\varepsilon\xi_1+\varepsilon^2\xi_2+\varepsilon^3\xi_3+\varepsilon^4\xi_4)}=e^{-\xi_0}-\varepsilon\xi_1e^{-\xi_0}+\frac{1}{2}\varepsilon^2(\xi_1^2-2\xi_2)e^{-\xi_0}\\&-\frac{1}{6}\varepsilon^3(\xi_1^3-6\xi_1\xi_2+6\xi_3)e^{-\xi_0}+\frac{1}{24}\varepsilon^4(\xi_1^4-12\xi_1^2\xi_2\\&+24\xi_1\xi_3+12\xi_2^2-24\xi_4)e^{-\xi_0}+O(\varepsilon^5)\end{aligned} \tag{B.4}$$

Hence, the asymptotic functions for the hyperbolic sine and cosine functions are

$$\begin{aligned}&\sinh(\xi_0+\varepsilon\xi_1+\varepsilon^2\xi_2+\varepsilon^3\xi_3+\varepsilon^4\xi_4)=\sinh\xi_0+\varepsilon\xi_1\cosh\xi_0\\&+\varepsilon^2(\xi_2\cosh\xi_0+\frac{1}{2}\xi_1^2\sinh\xi_0)+\varepsilon^3[(\frac{1}{6}\xi_1^3+\xi_3)\cosh\xi_0\\&+\xi_1\xi_2\sinh\xi_0]+\varepsilon^4[(\frac{1}{2}\xi_1^2\xi_2+\xi_4)\cosh\xi_0+(\frac{1}{24}\xi_1^4\\&+\frac{1}{2}\xi_2^2+\xi_1\xi_3)\sinh\xi_0]+O(\varepsilon^5)\end{aligned} \tag{B.5}$$

$$\begin{aligned}&\cosh(\xi_0+\varepsilon\xi_1+\varepsilon^2\xi_2+\varepsilon^3\xi_3+\varepsilon^4\xi_4)=\cosh\xi_0\\&+\varepsilon\xi_1\sinh\xi_0+\varepsilon^2(\xi_2\sinh\xi_0+\frac{1}{2}\xi_1^2\cosh\xi_0)\\&+\varepsilon^3[(\frac{1}{6}\xi_1^3+\xi_3)\sinh\xi_0+\xi_1\xi_2\cosh\xi_0]+\varepsilon^4[(\frac{1}{24}\xi_1^4\\&+\frac{1}{2}\xi_2^4+\xi_1\xi_3)\cosh\xi_0+(\frac{1}{2}\xi_1^2\xi_2+\xi_4)\sinh\xi_0]+O(\varepsilon^5)\end{aligned} \tag{B.6}$$